


# The interplay of internal and forced modes of Hadley Cell expansion: lessons from the global warming hiatus

Dillon J. Amaya<sup>1</sup>  · Nicholas Siler<sup>1</sup> · Shang-Ping Xie<sup>1</sup> · Arthur J. Miller<sup>1</sup>

Received: 30 June 2017 / Accepted: 16 September 2017 / Published online: 20 September 2017  
© Springer-Verlag GmbH Germany 2017

**Abstract** The poleward branches of the Hadley Cells and the edge of the tropics show a robust poleward shift during the satellite era, leading to concerns over the possible encroachment of the globe’s subtropical dry zones into currently temperate climates. The extent to which this trend is caused by anthropogenic forcing versus internal variability remains the subject of considerable debate. In this study, we use a Joint EOF method to identify two distinct modes of tropical width variability: (1) an anthropogenically-forced mode, which we identify using a 20-member simulation of the historical climate, and (2) an internal mode, which we identify using a 1000-year pre-industrial control simulation. The forced mode is found to be closely related to the top of the atmosphere radiative imbalance and exhibits a long-term trend since 1860, while the internal mode is essentially indistinguishable from the El Niño Southern Oscillation. Together these two modes explain an average of 70% of the interannual variability seen in model “edge indices” over the historical period. Since 1980, the superposition of forced and internal modes has resulted in a period of accelerated Hadley Cell expansion and decelerated global warming (i.e., the “hiatus”). A comparison of the change in these modes since 1980 indicates that by 2013 the signal has emerged above the noise of internal variability in the Southern Hemisphere, but not in the Northern Hemisphere, with the latter also exhibiting strong zonal asymmetry, particularly in the North Atlantic. Our results highlight the important interplay of internal and forced modes of tropical width change and

improve our understanding of the interannual variability and long-term trend seen in observations.

**Keywords** Hadley Cell expansion · Global warming hiatus · El Niño Southern Oscillation · Pacific Decadal Oscillation · Internal variability · Global climate model

## 1 Introduction

Recent studies have shown a significant expansion of the tropics since 1980 in a variety of observational products (e.g., Hu and Fu 2007; Fu and Lin 2011; Davis and Rosenlof 2012; Nguyen et al. 2013). This widening has been indicated by poleward displacements of the Hadley Cells (Hu and Fu 2007), subtropical dry zones (e.g., Sousa et al. 2011; Hoerling et al. 2012), extratropical storm tracks (Bender et al. 2012), and jet streams (Archer and Caldeira 2008). Such a major shift in global circulation and precipitation patterns has had a profound impact on communities and ecosystems found at the poleward margins of the subtropical dry zones, including higher occurrences of droughts in southern portions of Australia (CSIRO 2012), the southwestern United States (Cayan et al. 2010), the Altiplano region of South America (Morales et al. 2012), the Mediterranean (Sousa et al. 2011; Hoerling et al. 2012), and northern China (Ye 2014). This has led to significant public concern over a possible large scale “desertification” of these typically mild climates, and widespread interest in understanding the mechanisms governing tropical expansion.

While there is a broad agreement that the tropics are expanding, the magnitude of expansion depends on how the tropical boundary is defined and the dataset used for the analysis (Davis and Rosenlof 2012; Lucas et al. 2014). One common measure is the latitude closest to the equator at

---

✉ Dillon J. Amaya  
djamaya@ucsd.edu

<sup>1</sup> Scripps Institution of Oceanography, University of California-San Diego, 9500 Gilman Drive #0206, La Jolla, CA 92093-0206, USA

which the mid-tropospheric mass stream function is equal to zero (i.e., where mass transport shifts from poleward to equatorward between the Hadley Cell and the Ferrel Cell). According to this metric, total observed expansion can range from 0.2 to 3.2 degrees latitude decade<sup>-1</sup> depending on the reanalysis product (Johanson and Fu 2009; Davis and Rosenlof 2012). Other measures of tropical width are based on changes in tropopause height, which can be independent of Hadley Cell variability (Seidel et al. 2008). The zonal mean tropopause is relatively flat in the tropics with a height of about 15 km, but it lowers moving poleward to about 11–13 km in the extratropics and about 9 km near the poles. Therefore, tropopause based edge metrics estimated from radiosonde (Seidel and Randell 2006) and reanalysis data (Davis and Birner 2013) have utilized subtropical height thresholds to estimate symmetric expansion to be between  $-0.5^\circ$  and  $3.1^\circ$  latitude decade<sup>-1</sup>. Additionally, surface observations of zonal mean precipitation minus evaporation ( $P - E$ ) have been used to define the edge of the tropics as the transition between the E dominated subtropics (which reside under the subsiding branch of the Hadley Cells) to the P dominated midlatitudes (i.e., the latitudes closest to the equator at which  $P - E = 0$ ). This method suggests tropical expansion trends of  $-0.7$  to  $2.5$  in different reanalysis products (Davis and Rosenlof 2012).

The wide range in the trend estimates listed here could be due to each metric's propensity to isolate discrete levels of the atmosphere that have varying observational coverage. As a result, some estimates based on reanalysis data are less constrained by observations than others, and they can be plagued by the biases and errors associated with the underlying model used in a given reanalysis product (Trenberth et al. 2001; Sterl 2004). Additionally, early estimates that utilized absolute thresholds (like tropopause height) may be biased high due to uniform tropopause rise as a result of global warming.

Previous studies point to two main causes of Hadley Cell expansion since 1980. First, climate models forced with the observed increase in greenhouse gases produce a tropical widening (Lu et al. 2008; Hu et al. 2013); however, the magnitude of the trend is generally underestimated relative to observations. This has led some to suggest that non-greenhouse gas forcings, (i.e., anthropogenic aerosols and stratospheric ozone) may also play a significant role (Kang et al. 2011; Allen et al. 2012; Min and Son 2013; Kovilakam and Mahajan 2015; Waugh et al. 2015; Allen and Ajoku 2016).

Second, other studies have pointed to the primary influence of natural variability (Garfinkel et al. 2015). For example, multi-decadal trends in the Northern and Southern Annular Modes are thought to be important, with expansion (contraction) during their positive (negative)

phases driven by shifts in mid-latitude gross static stability (Previdi and Liepert 2007; Kang et al. 2011; Nguyen et al. 2013). Other studies have pointed to the importance of the El Niño–Southern Oscillation (ENSO) and the Pacific Decadal Oscillation (PDO), with contraction (expansion) of the Hadley Cell occurring during periods when SSTs in the tropical eastern Pacific are warm (cool) (Lu et al. 2008; Grassi et al. 2012; Allen et al. 2014; Lucas and Nguyen 2015; Mantsis et al. 2017; Allen and Kovilakam 2017). Lucas and Nguyen (2015) used radiosonde data and partial regression techniques to conclude that the 1980–2013 PDO phase change may account for as much as 50% of the widening over Asia, while Allen and Kovilakam (2017) used tropical Pacific pacemaker experiments to suggest unforced decadal ENSO variations can account for nearly all of the Northern Hemisphere (NH) zonal mean expansion and much of the Southern Hemisphere (SH) trend.

Disentangling the natural and forced contributions to Hadley Cell variability and expansion with such a limited observational record is a difficult task. These limitations are further compounded when taking into account the tendency of current width metrics to sample single levels of the atmosphere without considering how the tropical edge might vary with height. In this study, we attempt to overcome these limitations by using targeted modeling experiments and developing an objective, multivariate estimate of Hadley Cell width variability over a range of latitudes and heights to investigate the interaction between natural and forced variability over the satellite era. We find that since 1980, the superposition of forced and internal variability has resulted in an unusual period of accelerated Hadley Cell expansion, drawing parallels to a similarly unusual phenomenon—the global warming hiatus (Fyfe et al. 2016). Furthermore, we find that the strength of the forced tropical expansion is not symmetric about the equator, with the signal already emerging above the noise in the zonal mean SH, but not the NH. Finally, we consider zonal variations, moving beyond most previous studies that focused on the zonal mean. We find that while the SH largely follows the zonal mean results, the NH displays significant zonal variations, particularly in the North Atlantic. Our results add to the mounting evidence that internal variability plays a significant role in observed tropical expansion and raises several interesting questions for future studies.

The rest of the paper is organized as follows. In Sect. 2, we outline the data and methods used in the analysis. In Sect. 3, we discuss the interplay of internal and forced modes of tropical width variability in the zonal mean, and then explore zonal variations in these interactions in Sect. 4. We conclude with a summary and discussion in Sect. 5.

## 2 Data and methods

### 2.1 Joint Empirical Orthogonal Function

To objectively analyze variability of the zonal mean overturning circulation at a variety of atmospheric levels, we calculated a Joint Empirical Orthogonal Function (EOF) from 60°S to 60°N using three parameters widely discussed in the tropical expansion literature: (1) The zonal mean meridional mass streamfunction (MMS) at 500mb (Eq. 1;  $\psi_{500}$ ), (2) The zonal mean height of the tropopause ( $Z_T$ ), and (3) The zonal mean precipitation minus evaporation ( $P - E$ ). The MMS was calculated as:

$$\psi(P, \phi) = \frac{2a \cos \phi}{g} \int_{P_0}^P [v] dp, \quad (1)$$

where  $a$  is the radius of the Earth,  $g$  is gravitational acceleration,  $\phi$  is latitude,  $P_0$  is the model's lowest pressure level, and  $v$  is the meridional wind component, with brackets denoting the zonal average. The tropopause was calculated using monthly mean data and defined according to the World Meteorological Organization (WMO) lapse rate definition (WMO 1957). We focus only on the annual mean (from July to the following June) in order to better represent variability that is symmetric about the equator. Anomalies were calculated by removing the long-term annual mean climatology from each variable. Before taking the EOF, each of the individual components were normalized by its Frobenius norm (i.e., the square root of its total variance) and combined into a single matrix. The results of the Joint EOF are three spatial patterns representing the leading modes of  $\psi_{500}$ ,  $[Z_T]$ , and  $[P - E]$  as a function of latitude, where the time variability for all three patterns is described by a single principle component (PC). Here we focus only on the leading EOF and PC, for reasons that will become apparent in Sect. 3. Results are consistent if the domain is extended to 90°S–90°N or if just the NH or SH is included in the Joint EOF.

There are four main advantages to calculating the Joint EOF of  $\psi_{500}$ ,  $[Z_T]$ , and  $[P - E]$ . First, the method draws out the leading modes of variability among the three parameters without any a priori assumptions about what those modes might look like. Second, each chosen variable is related to a common Hadley Cell edge index found in the literature (Lucas et al. 2014). Third, the parameters represent horizontal slices at different pressure levels, which allows us to sample Hadley Cell variability throughout the troposphere without constraining our analysis to a single pressure surface. Finally, the Joint EOF identifies the modes when  $\psi_{500}$ ,  $[Z_T]$ , and  $[P - E]$  vary in tandem, and maximizes the signal by cutting down on unrelated noise present in

the individual parameters. When an EOF is taken for each individual parameter, the resulting spatial pattern tends to be a linear combination of the first and second Joint EOFs (not shown), which muddles the physical interpretation of the mode. Therefore, the Joint EOF method is the preferred method of isolating modes of variability in the zonal mean overturning circulation variability.

### 2.2 GCM experiments and observational datasets

We utilize two different experiments from the Geophysical Fluid Dynamics Laboratory climate model version 2.1 (GFDL-CM2.1) to separate and analyze natural and forced tropical width variability. First, natural variability is investigated using the 1000-year pre-industrial control simulation with all atmospheric forcings set to 1860 levels. Second, a 20-member historical all-forcing experiment from January 1861 to December 2014 is used to approximate the forced response. The historical ensemble includes 10-members from the CMIP5 archive and an additional 10-members run by Kosaka and Xie (2016). These experiments were initialized from a 600-year control and were forced with observed atmospheric forcings until 2006, and the RCP4.5 projected emissions scenario thereafter. CM2.1 has a resolution of approximately 2° latitude  $\times$  2.5° longitude with 17 vertical levels. The detailed formulation of CM2.1 has been documented by Delworth et al. (2006), and additional information regarding the additional 10-member historical ensemble and the control simulation can be found in Kosaka and Xie (2016).

For observations, we use the National Oceanic and Atmospheric Administration's (NOAA) Extended Reconstructed SST versions 3b (ERSSTv3b; Smith et al. 2008), and atmospheric temperature, wind velocity, precipitation and evaporation from the Modern Era Retrospective-analysis for Research and Applications 2 (MERRA2; Gelaro et al. 2017). The net effective radiative climate forcing from 1880 to 2012 was taken from Hansen et al. (2011), and is available at <http://www.columbia.edu/~mhs119/EnergyImbalance/Imbalance.Fig01.txt>.

## 3 Internal and forced modes of tropical width variability

### 3.1 Internal mode

We begin with the internal mode, which explains 49% of the total interannual variance across the three parameters within the pre-industrial control simulation. The climatology of  $\psi_{500}$  (black line) in Fig. 1a shows large positive (negative) values north (south) of the equator, representing the poleward branches of the NH and SH Hadley Cells. These

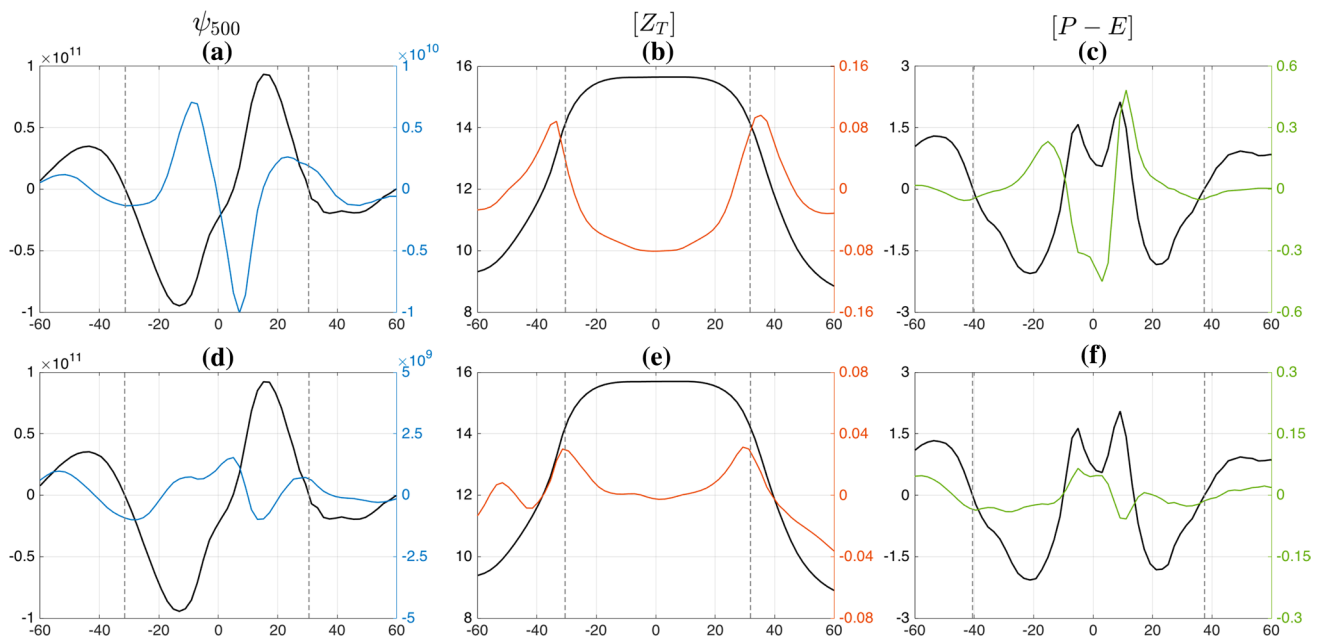


**Fig. 1** Joint EOF of  $\psi_{500}$  ( $\text{kg m}^{-1} \text{s}^{-1}$ ),  $[Z_T]$  (km), and  $[P-E]$  ( $\text{mm day}^{-1}$ ) in the 1000-year control simulation (top row) and the low-passed ensemble mean of the 20-member all-forcing historical simulation from 1861 to 2014 (bottom row). Black lines represent the zonal mean climatology of  $\psi_{500}$ ,  $[Z_T]$ , and  $[P-E]$ , respec-

tively. Colored lines are the EOF spatial patterns. Note that we have removed the tropical mean ( $15^\circ\text{S}$ – $15^\circ\text{N}$ ) from the  $[Z_T]$  anomalies to better assess the tropical edges without the influence of globally uniform tropopause rise

terminate around  $30^\circ$  as zero crossings in either hemisphere ( $\psi_{500} = 0$ ; vertical dashed lines), which is often defined to be the “edge” of the tropics (e.g., Lucas et al. 2014). Superimposed on the climatology is the leading internal mode of  $\psi_{500}$  variability (blue line). This mode features anomalies that are a near mirror-image about the equator, with two opposite-signed peaks in each hemisphere. The peaks correspond to negative (positive) anomalies on the equatorward flanks of the NH (SH) climatological Hadley Cell and positive (negative) anomalies on the poleward flanks. Note that the anomalies are slightly larger in magnitude in the NH than in the SH.

A similar pattern is seen in the leading internal mode for the other two parameters (Fig. 1b, c). The  $[Z_T]$  climatology (black line) depicts a maximum tropopause height in the tropics of about 15.5 km, dropping to about 9 km near  $60^\circ$  in either hemisphere. The tropical edge is similarly marked, but in this case as the latitude where the tropopause is 1.5 km less than the tropical ( $15^\circ\text{S}$ – $15^\circ\text{N}$ ) mean (i.e.,  $\Delta Z_T = 1.5$  km; Davis and Rosenlof 2012). Here the EOF shows positive anomaly peaks that slightly favor the NH (orange line), while a broad region of negative anomalies prevails within the tropics (Fig. 1b). Finally, the climatology of  $[P-E]$  shows two peaks, indicative of a double-ITCZ (Fig. 1c, black line). Poleward of these rain bands, there are regions of negative values in the subtropics associated with the descending branch of the climatological Hadley

Cell. The subtropical dry zones end with zero crossings around  $40^\circ$  in both hemispheres ( $[P-E]=0$ ), indicating a transition to mid-latitude storm tracks. The leading internal mode in  $[P-E]$  shows positive anomalies poleward of the model’s ITCZ climatological peaks and negative anomalies from  $10^\circ\text{S}$ – $10^\circ\text{N}$  that are nearly symmetric about the equator, along with negative anomalies at the subtropical edges overlying the climatological zero crossings.

In each case, the leading Joint EOF projects strongly in the tropics and in tropical edge regions traditionally captured by the various edge indices outlined in the literature (vertical dashed lines). Further, the sign of the anomalies and their meridional positions are all consistent with a poleward expansion of each parameter’s climatological tropics. This is highlighted by the high correlation between the associated internal mode PC ( $\text{PC}_{\text{int}}$ ; purple line Fig. 2a) and individual total (NH + SH) tropical edge indices ( $R=0.75$ ,  $R=0.94$ , and  $R=0.71$  for  $\psi_{500} = 0$ ,  $\Delta Z_T = 1.5$  km, and  $[P-E] = 0$ , respectively). In contrast, PCs from the next four EOFs do not project as strongly on these edge indices, and tend to have average correlation coefficients of less than 0.2 (not shown). Thus, the leading internal mode can be confidently interpreted as a measure of internal tropical width variability, and we will not focus on higher order modes as a result.

$\text{PC}_{\text{int}}$  is strongly correlated with the Nino3.4 index ( $R = -0.96$ ; black line), indicating that its variability is primarily driven by ENSO (Fig. 2a). The negative sign of the



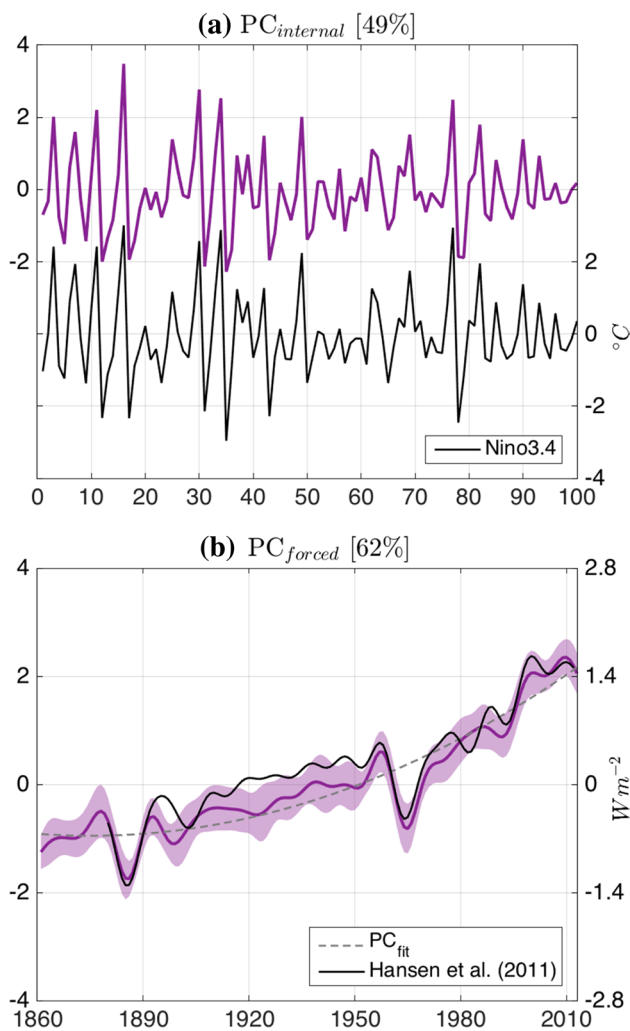


**Fig. 2**  $PC_{\text{for}}$  and  $PC_{\text{int}}$ , respectively. Numbers in square brackets are the percent variance explained by each EOF mode among the three variables in Fig. 1. Black line in **a** is the control simulation Nino3.4 index ( $^{\circ}\text{C}$ ). For clarity, only the first 100 years of  $PC_{\text{int}}$  and Nino3.4 are shown. Gray dashed line in **b** is second-order least-squares fit to  $PC_{\text{for}}$ . Black line in **b** is the net effective climate forcing taken from Hansen et al. (2011) ( $\text{Wm}^{-2}$ )

correlation indicates that high values of  $PC_{\text{int}}$  correspond to a La Niña-like pattern. These results are consistent with several studies showing that a La Niña anomalously weakens the thermally driven subtropical jet stream, shifting eddy-momentum convergence and the meridional circulation poleward (Robinson 2002; Seager et al. 2003; Lu et al. 2008).

### 3.2 Forced mode

We now focus on the forced mode, which represents the Joint EOF within the ensemble mean of 20 GFDL-CM2.1 historical all-forcing simulations, and explains 62% of the total interannual variance (Fig. 1, bottom row). Averaging across the ensemble reduces random internal variability,

thereby enhancing the signal of the forced response. In addition, each parameter was first linearly detrended, subjected to a 10-year low-pass filter, and then retrended before calculating the EOF, further minimizing the influence of internal variability.

The PC for the forced mode ( $PC_{\text{for}}$ ) is characterized by a long-term secular trend from 1860 to 2013 that is intermittently punctuated by strong negative peaks (Fig. 2b).  $PC_{\text{for}}$  is highly correlated with the low-passed net effective climate forcings at the top of the atmosphere (TOA) from 1880 to 2012 derived from Hansen et al. (2011) (black line;  $R=0.97$ ;  $R=0.85$  detrended). Therefore, these negative peaks could be due to strong volcanic forcing, while the long-term trend may be attributed to increased greenhouse gases and decreased stratospheric ozone concentration throughout the historical period, which is supported by the high correlation between low-passed global mean SST (GMSST) and  $PC_{\text{for}}$  ( $R=0.98$ ;  $R=0.89$  detrended). Similar to  $PC_{\text{int}}$ ,  $PC_{\text{for}}$  also projects strongly on low-passed variability at the edge of the tropics, with raw (detrended) correlations of  $R=0.98$  (0.88),  $R=0.91$  (0.70), and  $R=0.93$  (0.72) for the total (NH + SH)  $\psi_{500} = 0$ ,  $\Delta Z_T = 1.5$  km, and  $[P - E] = 0$  edge indices, respectively. The high correlation of  $PC_{\text{for}}$  with TOA radiative forcings, GMSST, and the traditional edge indices gives us confidence that the Joint EOF method is credibly capturing the time variability and trend associated with the prescribed external forcing of the zonal mean overturning circulation in this model.

The forced EOFs spatial patterns (Fig. 1d–f) have several similarities to their internal counterparts (Fig. 1a–c). For example, in all three parameters there are forced anomalies of the same sign as the internal anomalies overlying the subtropical zero crossings of the  $\psi_{500}$  and  $[P - E]$  climatology and near the regions where  $\Delta Z_T = 1.5$  km. This suggests that the forced mode induces a similar poleward expansion of the climatological Hadley Cells, tropical tropopause heights, and subtropical dry zones as the internal mode. However, while the internal mode anomalies are slightly larger in the NH, there is an asymmetry in the magnitude of the forced anomalies in favor of the SH. Uniform forcings like greenhouse gas emissions influence the tropics nearly equally between hemispheres (Lu et al. 2008; Seager et al. 2010; Hu et al. 2013), but an asymmetric forcing like ozone may explain the enhanced SH tropical expansion in our forced EOF mode (Kang et al. 2011; Polvani et al. 2011b; Min and Son 2013; Lucas and Nguyen 2015). Anthropogenic aerosols are another asymmetric forcing (Wang et al. 2016) that have been hypothesized to contribute to Hadley Cell expansion (Allen et al. 2014), but modeling studies have indicated the ozone effect dominates the SH zonal mean response (Tao et al. 2016).

### 3.3 Mode interactions: total variance and total expansion

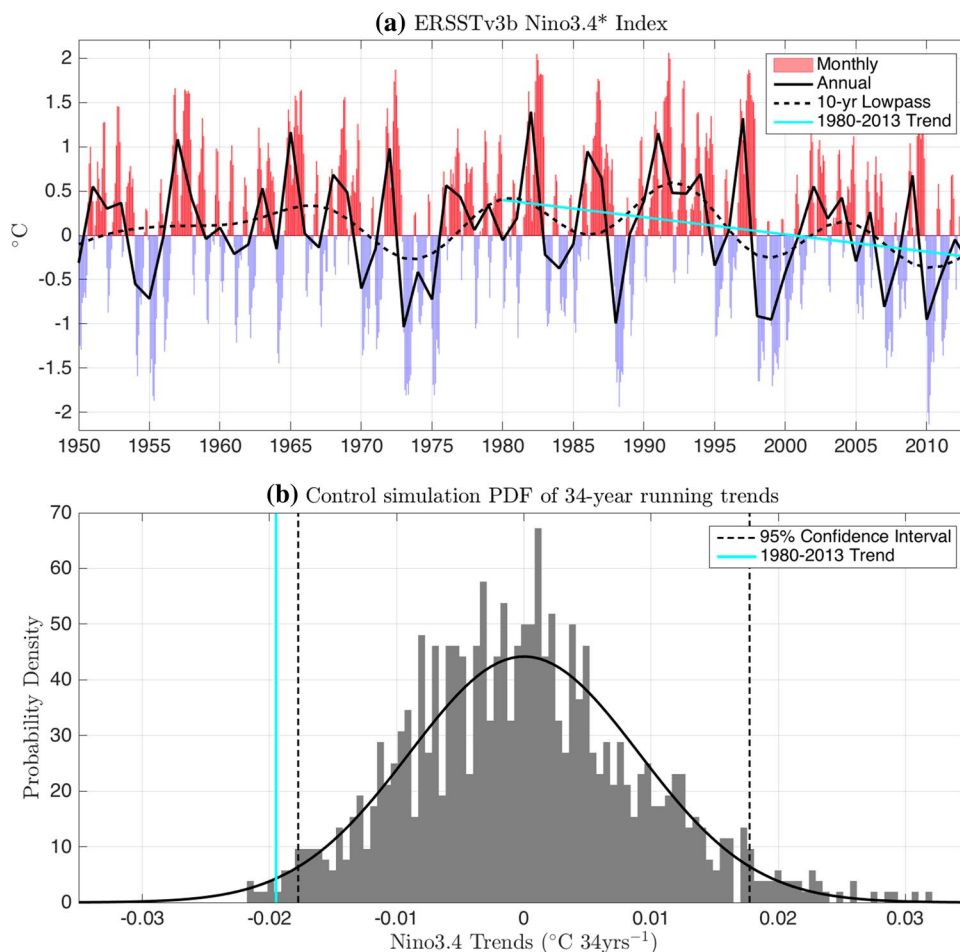
To what degree can the forced and internal modes represent the total tropical width variance? To test this, we project each ensemble member of the historical simulation onto the internal and forced EOF patterns to acquire two PCs that represent the time variability of the leading modes of forced and internal tropical width changes in each member. We then construct a multivariate linear regression model for each member based on the regression coefficients between these two PCs and the traditional edge indices discussed previously. We are then able to compare the results of this model to the total (NH + SH) traditional edge indices in each member. Using this method, we find that the combination of our two EOF modes can explain  $66 \pm 4$ ,  $85 \pm 2$ , and  $57 \pm 5\%$  of the total unfiltered variance in  $\psi_{500} = 0$ ,  $\Delta Z_T = 1.5$  km, and  $[P - E] = 0$ , respectively. This result supports the conclusions of recent studies that ENSO and external forcings are the primary drivers of interannual tropical width variability in the zonal mean (Allen et al. 2014; Mantsis et al. 2017; Allen and Kovilakam 2017). Recall, however, that our Joint EOF method does not partition the influence of the different

external forcings on Hadley Cell width (i.e., ozone and/or greenhouse gases). As such, single forcing experiments that take advantage of this objective methodology are needed in future studies to further quantify the role of these individual drivers in Hadley Cell width variability.

A related question is, how much of the observed changes in tropical width during the satellite era can be attributed to these modes? To answer this, we first scale the EOFs by the observed changes in each PC from 1980 to 2013, and then add the results to the climatology of each parameter to measure how far the climatological tropical edges (vertical dashed lines) shift poleward. The scaling required for the forced EOF is fairly straightforward in that it is the change in  $PC_{for}$  from 1980 to 2013 due to the trend, which we estimate to be  $1.31\sigma$  using a 2nd-order polynomial fit to the entire time series.

The scaling for the internal mode is based on the regression coefficient between  $PC_{int}$  and Nino3.4 ( $R_{coeff} = -0.94 \sigma^\circ C^{-1}$ ). Using observed SST from ERSSTv3b, we produce a Nino3.4\* index (Chen and Wallace 2015), and calculate the linear trend from 1980 to 2013 based on the 10-year low-passed time series ( $-0.66^\circ C$  over 34 years; Fig. 3a). This trend is multiplied by  $R_{coeff}$  to get an estimate for the

**Fig. 3** **a** Monthly mean Nino3.4\* index calculated from ERSSTv3b ( $^\circ C$ , red/blue shading). Black solid line is the annual mean, black dashed line is the 10-year low-pass filter, and cyan line is the linear fit from 1980 to 2013. **b** Probability density function (PDF; gray shading) of 34-year running trends of Nino3.4 in a 1000-year control simulation. Black solid line following gray shading is a Gaussian distribution with the same mean and standard deviation as the PDF. Black dashed lines mark 95% confidence intervals. Vertical cyan line represents the observed trend (a). Note the height of the cyan line is arbitrary



representative scaling in  $PC_{int}$  ( $0.63\sigma$ ). The fact that the scaling is less than  $1\sigma$  makes sense because the internal mode is the result of interannual variability and we are interested in a representative multi-decadal trend in these anomalies. This does not mean, however, that the observed trend in Nino3.4\* is so common. On the contrary, by calculating a 34-year running trend time series in the control simulation Nino3.4, we put the observed Nino3.4\* trend into historical context and find that it was actually quite extreme ( $\sim 2.12\sigma$ ) relative to the probabilistic range of 34-year trends that may be expected in nature (Fig. 3b).

The strong cooling observed in the Nino3.4\* index has been linked to a decadal strengthening of the tropical Pacific trade winds (e.g., Watanabe et al. 2014; Amaya et al. 2015), and this acceleration may be the result of aerosol forcing (Takahashi and Watanabe 2016). Therefore, it is possible that the trend in Fig. 3b is also partially forced by aerosols. However, Allen and Kovilakam (2017) recently used the CMIP5 ensemble to show that forced SST patterns only weakly project on eastern tropical Pacific during this time period. Thus, we continue under the assumption that cooling trend in Fig. 3b is entirely due to internal variability, but we acknowledge that further research is needed to quantify the role of external forcings on tropical Pacific SST trends. These results will be discussed in greater detail in Sect. 5.

The contributions of the scaled anomalies to tropical expansion are reported in Table 1 as changes in degrees latitude. Based on the combination of the two Joint EOFs, we estimate a total NH expansion of  $0.26^\circ$ ,  $0.55^\circ$ , and  $0.38^\circ$  latitude and a total SH expansion of  $0.38^\circ$ ,  $0.44^\circ$ , and  $0.35^\circ$  latitude for  $\psi_{500}$ ,  $[Z_T]$ , and  $[P - E]$ , respectively. Interestingly, the internal anomalies account for 58, 73, and 63% of the overall NH change in each parameter, but only 42, 66, and 40% of the SH expansion. This is generally consistent with Allen and Kovilakam (2017) and others, who suggest that NH tropical expansion is dominated by unforced trends due to ENSO. These model expansion estimates are smaller than most other observational estimates during the same time period, which could be due in part to observational uncertainty (Lucas et al. 2014), or a broader problem with coupled

models underestimating the observed tropical expansion (Hu et al. 2013; Tao et al. 2016).

The fact that the expansion of the NH Hadley Cell in the model is primarily driven by natural variability during the satellite era could be due to the differences in the strength of the two EOFs near the tropical edges (note the change in y-axis between top/bottom row of Fig. 1). The internal anomalies are stronger than the forced anomalies in these regions, particularly in the NH, which is possibly a consequence of the observed asymmetrical strength of ENSO teleconnections to the NH relative to the SH (Garreaud and Battisti 1999). In contrast, the forced anomalies tend to be stronger near the SH tropical edge, which is likely due to the presence of asymmetric forcings such as ozone (Tao et al. 2016). This inverse asymmetry between the two modes leads to a larger difference in the magnitude of internal and forced anomalies near the NH tropical edge and a smaller difference near the SH tropical edge for a  $1\sigma$  occurrence/trend of both EOFs. Therefore, on short time scales when the trend in  $PC_{for}$  is small, we expect that anthropogenic expansion of the NH Hadley Cell would be dominated by natural variability.

### 3.4 Mode interactions: signal time of emergence in the zonal mean

On long time scales, it is interesting to consider the time when the anomalies associated with the forced expansion of the Hadley Cell rise above the noise level of the internal mode. Since we are interested in multi-decadal Hadley Cell expansion over the satellite era, we will focus on the time of emergence of the forced trend beginning in 1980. This trend is estimated with a 2nd-order least-squares fit ( $PC_{fit}$ ; Fig. 2b) calculated from 1861 to 2013, and is extrapolated into the future until the signal is sufficiently large (see next paragraph). The trajectory of  $PC_{fit}$  corresponds to a non-equilibrium  $2.0^\circ\text{C}$  increase in GMSST by 2100 ( $3.0^\circ\text{C}$  for global mean surface temperature; GMST), which roughly corresponds to the CMIP5 RCP6.0 future warming scenario (Stocker et al. 2013).

Here we define the time of signal emergence to be the year when the forced trend in each parameter is significantly larger than the probabilistic range of unforced trends in Hadley Cell width due to  $PC_{int}$ . This condition is met when:

$$\alpha_k R(\phi_{TE})_{for} > \sigma_k t_{0.95} R(\phi_{TE})_{int} \quad \text{for } k = 2, 3, 4, \dots, n, \tag{2}$$

where  $\phi_{TE}$  is the latitude of the climatological tropical edge defined by the traditional edge indices,  $\alpha_k$  is the  $k$ -year change in  $PC_{fit}$  from 1980 to  $k - 1$  years after 1980,  $R_{for}$  ( $R_{int}$ ) is the regression slope at  $\phi_{TE}$  of each respective parameter in the EOF onto  $PC_{for}$  ( $PC_{int}$ ),  $\sigma_k$  is the standard deviation of a  $k$ -year running trend of  $PC_{int}$ , and  $t_{0.95}$  is the t-statistic for a 95% confidence interval based on the  $k$ -year running

**Table 1** Total (NH+SH) tropical expansion ( $^\circ$ latitude) based on scaled anomalies in Fig. 1

Metric	Internal 1980–2013	Forced 1980–2013	Internal + forced 1980–2013
$\psi_{500}$	NH: 0.15	NH: 0.11	NH: 0.26
	SH: 0.16	SH: 0.22	SH: 0.38
$[Z_T]$	NH: 0.40	NH: 0.15	NH: 0.55
	SH: 0.29	SH: 0.15	SH: 0.44
$[P - E]$	NH: 0.24	NH: 0.14	NH: 0.38
	SH: 0.14	SH: 0.21	SH: 0.35

trend time series. Thus, if the magnitude of the forced trend exceeds the 95% confidence level for  $k$ -year running trend time series, then we consider the signal to have emerged above the “noise” of  $PC_{int}$  (i.e., ENSO-like variability). If the magnitude of the forced trend is not significant, then we increase  $k$  and repeat the process.

Since these Joint EOF patterns primarily describe the expansion of the Hadley Cells, we report the time of emergence for forced anomalies at the tropical edges (i.e., at the latitudes of the vertical dashed lines in Fig. 1). Within this framework, we find that the zonal mean forced anomalies contributing to SH Hadley Cell expansion emerge above the ENSO-driven noise level at 95% confidence in 2007, 2010, and 2003 for  $\psi_{500}$ ,  $[Z_T]$ , and  $[P - E]$ , respectively. In contrast, the forced anomalies contributing to NH Hadley Cell expansion do not rise above the noise until 2019, 2015, and 2023. This is consistent with our previous results indicating that forced Hadley Cell variability is larger in the SH than in the NH. It also implies that, in the zonal/annual mean and to the extent that ENSO represents the dominant form of “noise”, anomalies that would contribute to externally forced Hadley Cell expansion over the satellite era may currently be detectible in the SH, while the forced expansion of the NH tropics may become apparent in the next decade based on the current trajectory of the forced trend. Other forms of internal variability produced by different climate modes or stochastic noise may also prove important, but can only delay the signal emergence further into the future for each hemisphere.

### 3.5 Hadley Cell expansion during hiatus periods

Based on the discussion of Figs. 1, 2 and 3, it is evident that both ENSO-like variability and external forcings play important roles in the year-to-year and long-term changes in tropical width. This conclusion draws interesting parallels between tropical expansion and the recent “hiatus” in global warming (e.g., Amaya et al. 2015; Kosaka and Xie 2016; Xie and Kosaka 2017). In particular, natural modulations of ENSO/PDO and long-term secular warming due to increased greenhouse gases linearly superimpose upon each other to reproduce the so-called global warming “staircase” and the early 2000’s global warming hiatus (e.g., Kosaka and Xie 2016).

Similarly, the leading internal mode shown in Fig. 1 suggests that ENSO variability also plays an important role in modulating tropical width, but in the opposite sense of global temperature, as illustrated in Fig. 4. Specifically, we hypothesize that decadal shifts between periods of predominantly El Niño events (red shading) to predominantly La Niña events (blue shading) will tend to produce long-term trends (such as in Fig. 3) that act to dampen forced GMST warming (red line), while simultaneously enhancing forced

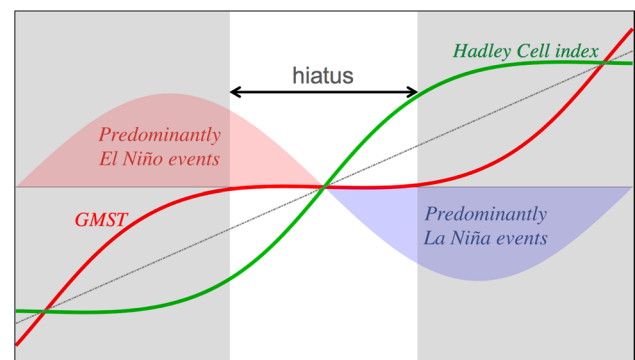


**Fig. 4** Schematic demonstrating the hypothesized interplay between anthropogenic forcings (gray dashed line) and decadal phases in the relative frequency of ENSO events (red/blue sine wave). Green line represents trajectory of a measured Hadley Cell edge index with time. Red line represents trajectory of measured global mean surface temperature (GMST) with time. During the long-term transition from a period of more El Niño events (red shading) to a period of more La Niña events (blue shading), forced global warming is dampened and the trend flattens out, producing a hiatus period. Simultaneously, the increasing prevalence of La Niña-forced Hadley Cell expansion drives accelerated widening of the tropics through an enhancement of the externally forced Hadley Cell widening

Hadley Cell expansion as measured by a traditional edge index (green line).

To test this hypothesis, we first show the 14-year trend over the observed “hiatus period” (2000–2013) in  $Nino_{3.4}^*$  and GMSST for each member of the GFDL-CM2.1 historical simulation (Fig. 5a). There are some members that have long-term cooling trends in  $Nino_{3.4}^*$  during this time period, while others have long-term warming trends. The spread in the trends is due to the presence of internal variability in each member, and the trends themselves represent random transitional periods between one phase of decadal ENSO variability to the other in the model. Ensemble members with larger warming (cooling) trends in  $Nino_{3.4}^*$  tend to have larger (smaller) GMSST warming trends than the ensemble mean (forced warming, dashed red line) during this time period ( $R = 0.74$ ). This is consistent with the red line in our schematic (Fig. 4) and with previous studies that have shown that long-term changes in ENSO can dampen or amplify forced warming trends (Kosaka and Xie 2013; Fyfe and Gillett 2014).

Figure 5b shows the same 14-year trends in GMSST, but compared to 14-year trends in the symmetric Hadley Cell index  $[P - E] = 0$ . In general, ensemble members with weaker GMSST warming trends tend to have Hadley Cells that are expanding more rapidly than the ensemble mean or forced expansion ( $R = -0.73$ ; horizontal red dashed line). This suggests that simulations with prolonged cooling in the equatorial Pacific are not only dampening global warming due to increased greenhouse gases, but are also enhancing the forced expansion of the tropics in the model. This result



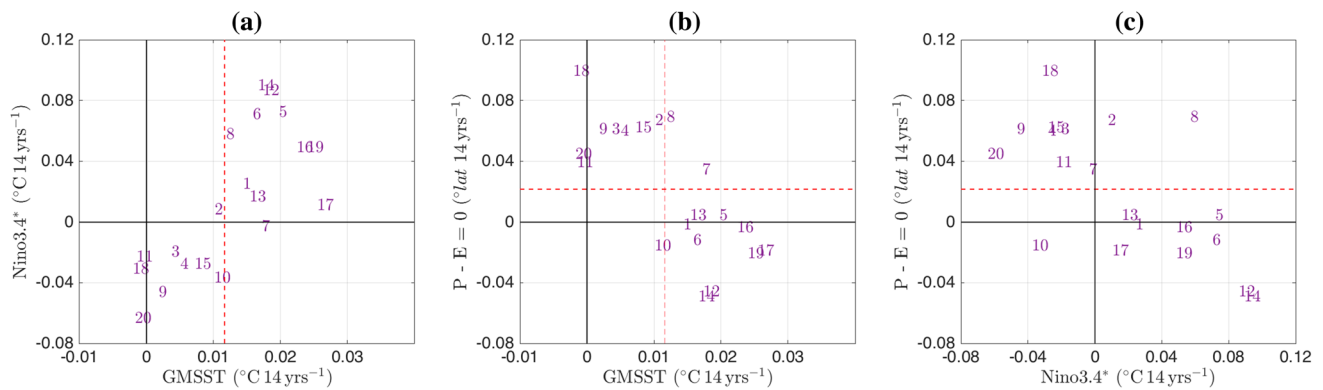


**Fig. 5** **a** Trends in Nino3.4\* ( $^{\circ}\text{C } 14 \text{ yrs}^{-1}$ ) versus trends in GMSST ( $^{\circ}\text{C } 14 \text{ yrs}^{-1}$ ). **b** Trends in the latitude where  $P-E=0$  ( $^{\circ}\text{lat } 14 \text{ yrs}^{-1}$ ) versus trends in GMSST. **c** Trends in the latitude where  $P-E=0$  versus trends in Nino3.4\*. Every trend is calculated

from 2000 to 2013. Different numbers represent different members of the 20-member all-forcing historical ensemble. Red dashed lines in each case are the ensemble mean trend for the corresponding axis

is further reinforced in by Fig. 5c, which shows the edge index trend versus the Nino3.4\* trend. Broadly, ensemble members with stronger cooling trends in Nino3.4\* have accelerated Hadley Cell expansion relative to the ensemble mean, and ensemble members with warming trends in Nino3.4\* have dampened forced expansion trends ( $R = -0.65$ ). Similar correlations are found among 14-year trends in GMSST, Nino3.4\*, and  $P-E$  over the full simulation period (1874–2013), giving us high confidence in their robustness.

#### 4 Zonally varying responses to Hadley Cell expansion

An important focus of recent literature has been on the regional characteristics of Hadley Cell expansion (Choi et al. 2014; Chen et al. 2014; Karlsruhas and Ummenhofer 2014; Lucas and Nguyen 2015). These studies have largely been based on radiosonde and satellite data, and they indicate that there may be significant differences in tropical expansion rates depending on the region of interest. In this section, therefore, we extend our EOF analysis to two dimensions, in order to better understand how internal and forced modes of Hadley Cell variability interact regionally.

##### 4.1 Zonal variations in $P-E$ and signal time of emergence

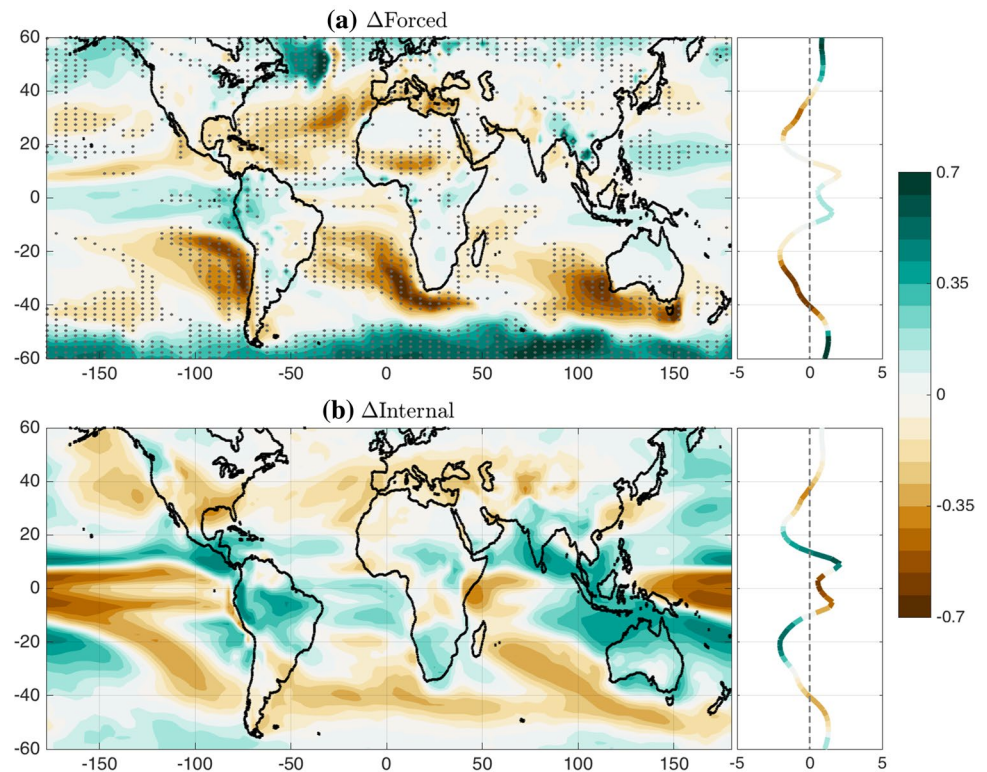
Figure 6a shows the regression of the low-passed ensemble mean  $P-E$  field onto  $PC_{\text{for}}$  scaled by the change in  $PC_{\text{fit}}$  from 1980 to 2013 ( $1.31\sigma$ ), which represents the  $P-E$  signal associated with forced tropical expansion in the model. Figure 6b shows the regression of the control simulation  $P-E$  field onto  $PC_{\text{int}}$ , scaled by the 95% confidence level for

34-year running trends ( $\sigma_{34}t_{0.95} = 0.63$ ; Eq. 2). In both cases, the regression pattern has been weighted by the standard deviation of the control simulation  $P-E$  at each grid point. The shape of the line in the side-panels of each subplot in Fig. 6 represents the zonal mean climatology of  $P-E$ . The color of the line represents the zonal mean regression of  $P-E$  with each respective PC, which has been weighted by the standard deviation of the zonal mean control simulation  $P-E$  at each latitude and scaled the same as the spatial map to its left.

The forced  $P-E$  regression (Fig. 6a) is characterized by a near-zonally uniform increase in  $P-E$  from  $50^{\circ}\text{S}$ – $60^{\circ}\text{S}$ , punctuated by smaller regions of strong  $P-E$  reduction in the Southeast Pacific, South Atlantic, and Southeast Indian Ocean, which are likely due to the poleward shift in the SH subtropical high centers in each basin (Karlsruhas and Ummenhofer 2014). This result is further highlighted by the negative zonal mean anomalies found at the climatological SH zero crossing of  $P-E$  (Fig. 6a, side-panel). A similar shift is evident in the NH, but with less zonal symmetry. In the North Atlantic, there is a strong increase in  $P-E$  at high latitudes coupled with a strong reduction in subtropical  $P-E$  that encompasses much of southern Europe and the Mediterranean Sea. This is consistent with the zonal mean expansion of the NH dry zones and long-term observations of the region (Hoerling et al. 2012). However, in the North Pacific, North America, and over the main Eurasian continent, the anomalies are much weaker, explaining the weaker zonal-mean regressions for the NH as a whole (side panel of Fig. 6a).

Figure 6b shows many of the defining characteristics of a La Niña event. In the tropical Indo-Pacific, there are anomalies consistent with a western shift and intensification of the Walker Circulation and the poleward shift in the zonal mean ITCZ and SPCZ seen in the Fig. 6b side-panel. In the

**Fig. 6** **a** Regression of ensemble mean  $P - E$  with  $PC_{\text{for}}$  scaled by change in  $PC_{\text{fit}}$  from 1980 to 2013. **b** Regression of control simulation  $P - E$  with  $PC_{\text{in}}$  scaled to represent a 95% confidence interval of 34-year running trends using Eq. (2). Both patterns weighted by standard deviation of control simulation  $P - E$  anomalies at each grid point. Shape of line in each side-panel is zonal mean climatological  $P - E$  as a function of latitude. Shading of each line right of **a** and **b** represents regression of zonal mean  $P - E$  with respective  $PC$ , scaled the same as corresponding  $x/y$  map. Stippling in **a** denotes grid points where signal has emerged above the noise by 2013 (see text)



North Pacific, there is a reduction in  $P - E$  throughout the southern portion of the United States, consistent with the Rossby wave train that tends to steer extratropical cyclones to higher latitudes during La Niña events (Horel and Wallace 1981). The North Atlantic, southern Europe, and Mediterranean also experience a drying associated with a poleward expansion of the Hadley Cell, a shift in the precipitation bands, and increased evaporation at the surface due to increased subsidence. As a result, the zonal mean regression of internal anomalies produces a poleward expansion of the NH subtropics with negative anomalies at the NH climatological  $P - E$  zero crossing (Fig. 6b, side-panel). In the SH subtropics, the anomalies are similar in space to the forced anomalies discussed in Fig. 6a, though their magnitudes are smaller. At high southern latitudes, there are hints of a poleward displacement of extratropical storm tracks with the South Pacific dominating the zonal mean.

Equation (2) was applied to each grid point to determine the year in which the  $P - E$  signal would rise above the noise. As a result, stippling in Fig. 6a indicates forced  $P - E$  changes that have emerged above the noise-level of  $PC_{\text{int}}$  at the 95% confidence level by 2013. Consistent with the results presented in Sect. 3.2, much of the SH  $P - E$  signal in the subtropics and high latitude Southern Ocean has emerged during the early parts of the twenty-first century. This once again emphasizes the tendency for the SH forced changes to follow the zonal mean. The bulk of NH forced anomalies over the subtropical latitudes of the North Pacific,

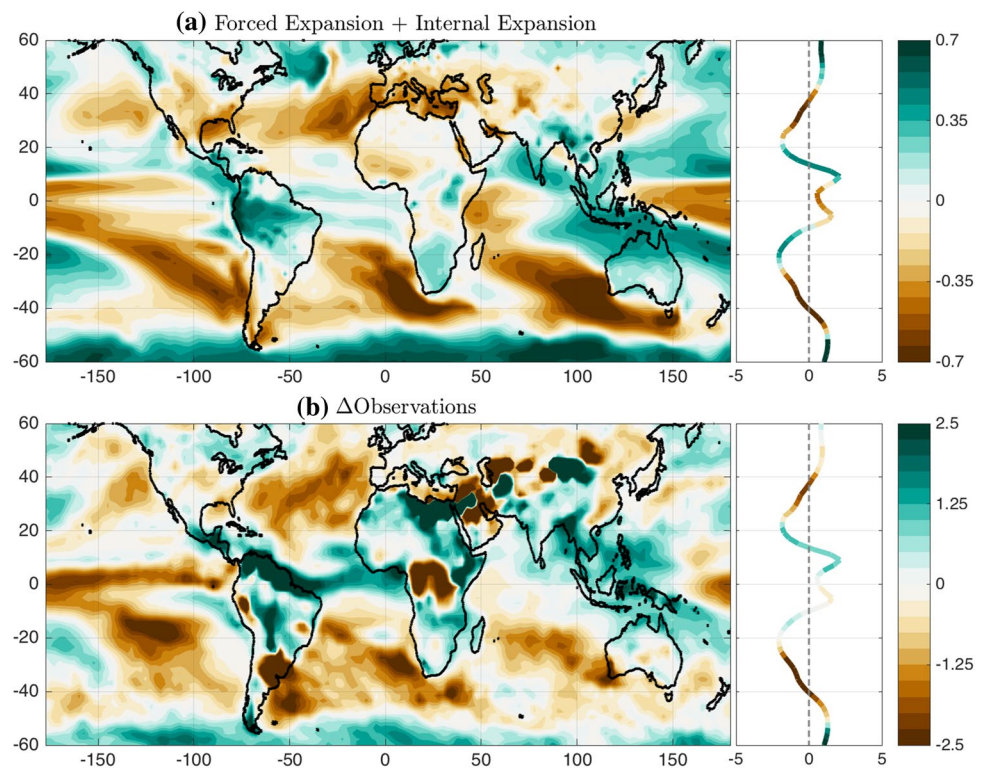
North America and Eurasia also follow the zonal mean results and remain below the noise threshold through 2013. The North Atlantic does not follow this pattern, but instead has a large proportion of forced changes (particularly at high latitudes) that are detectable by 2013. This result stands in contrast to the zonal mean view of Hadley Cell expansion discussed earlier and highlights the importance of a regionally varying perspective, particularly with respect to future atmospheric forcings.

#### 4.2 Zonally varying mode interactions with observational comparisons

Next, we further analyze any zonal variations in the interaction between the internal and forced modes of Hadley Cell width change during the satellite record (Fig. 7a). In accordance with the schematic outlined in Fig. 4, we scale the forced  $P - E$  regression pattern by the same change in  $PC_{\text{fit}}$  from 1980 to 2013 as before ( $1.31\sigma$ ), and then calculate linear a combination of this pattern with the internal mode  $P - E$  regression scaled by the observed change in  $Nino3.4^*$  during the same time period (i.e.,  $0.63\sigma$ ; see Sect. 3.3). This exercise allows us to consider the linear enhancement of forced  $P - E$  changes from 1980 to 2013 by the observed decadal shift from predominantly El Niño events to predominantly La Niña events (Figs. 3, 4, 7a).

Generally, the internal  $P - E$  anomalies dominate the mode superposition throughout the tropics, North America,

**Fig. 7** **a** The sum of Fig. 6a, b. Figure 6b was first scaled by the observed change in Niño3.4\* from 1980 to 2013 before performing taking the sum (see text). **b** Regression of observed annual mean P–E with composite Hadley Cell edge index from 1980 to 2013, scaled by the change in the composite edge index over this time period (2.27 °lat). Note the different colorbars. Regressions are weighted by the standard deviation of control simulation P–E anomalies at each grid point



and Eurasian continent (Fig. 7a). However, in regions where the forced anomalies project strongly (i.e., the North Atlantic and SH), the interactions between the modes can be important. For example, the subtropical North Atlantic and Mediterranean regions experience a sharp decrease in P–E as the two modes enhance one another. In the zonal mean, the anomalies found at the NH climatological zero crossing experience a similar strengthening (Fig. 7a, side-panel). This enhancement is consistent with our earlier results that showed a larger poleward shift of the dry zone edges when the impacts of the internal mode and forced mode “line-up” (Figs. 4, 5). SH anomalies experience a similar regional and zonal mean intensification with more negative (positive) P–E anomalies throughout the subtropics (high-latitudes) relative to either the internal mode or forced mode individually.

Previous studies have indicated that a combination of anthropogenic forcings and decadal ENSO variations such as in Fig. 7a can account for most of the observed tropical expansion during the satellite era (Grassi et al. 2012; Allen et al. 2014; Lucas and Nguyen 2015; Mantsis et al. 2017; Allen and Kovilakam 2017). We further test this hypothesis in the zonally varying sense by comparing Fig. 7a to observed P–E changes associated with observed Hadley Cell width variability. Figure 7b shows the observed regression pattern of annual mean MERRA2 P–E fields with a composite Hadley Cell edge index from 1980 to 2013, weighted by the control simulation P–E standard

deviation at each grid point. The composite edge index was taken as the average of three observed total (NH + SH) annual mean edge indices discussed earlier ( $\psi_{500} = 0$ ,  $\Delta Z_T = 1.5$  km, and  $[P - E] = 0$ ). We combine the indices in this way to get a more robust estimate of the variability and long-term trend in Hadley Cell width, which can vary substantially from one index to another (e.g., Lucas et al. 2014). As in Fig. 7a, the regression pattern was then scaled by the observed trend in the composite index over the 34-year period (2.27° latitude) to represent the change in weighted P–E over this time period. Our results are generally consistent using any individual index for the regression.

Broadly, the EOF reconstruction and the observed P–E changes share much of the same large-scale features. Both patterns have a near-zonally uniform P–E increase at high southern latitudes, as well as remarkably consistent pockets of SH subtropical drying. In the NH, they also show a similar decrease in P–E in the northeast Pacific off the coast of California and a much stronger P–E reduction throughout the North Atlantic and Mediterranean Sea (Bender et al. 2012; Hoerling et al. 2012). The observations also show the Indo-Pacific zonal gradient in P–E that is reminiscent of La Niña-like conditions. All told, we contend that the two patterns are qualitatively quite similar, which further supports the hypothesis that atmospheric forcings and decadal ENSO transitions can explain much of the observed change in tropical width.



Repeating the experiment with different reanalysis products generates similar regression patterns to Fig. 7b, but the magnitude of the trend in each composite edge index (i.e. the scaling of Fig. 7b) varies substantially. For example, data taken from the National Center for Environmental Programs Reanalysis 2 (NCEP2) produces a 34-year expansion of less than 1 degree latitude (not shown). As a result, it would appear that the spatial pattern seen in Fig. 7b is robust, but as currently scaled the magnitude of anomalies may be overestimated as the MERRA2 trend is on the higher end of observational estimates (Lucas et al. 2014). Therefore, despite the EOF reconstruction appearing much weaker than MERRA2 (note the colorbar change), Fig. 7a falls within the range of observational uncertainty. The good agreement between our results and observations implies that the satellite record just so happens to correspond with a period of accelerated tropical expansion akin to the accelerated warming periods of the 1970s–1990s (Kosaka and Xie 2016). Indeed, if not for the decadal La Niña-like cooling pattern in the tropical Pacific the observed trend may have been substantially smaller.

## 5 Summary and discussion

In this study, we sought to identify the leading modes of internal and forced tropical width variability without any *a priori* assumptions about what those modes might look like. Using a Joint EOF approach, we found that the leading internal mode is closely associated with ENSO variability, the leading forced mode is related to TOA radiative forcings, and each mode is characterized by symmetric poleward expansion of the climatological Hadley Cells. The forced EOF showed an asymmetry in favor of enhanced SH tropical expansion relative to the NH. This is possibly due to asymmetric ozone forcing (Kang et al. 2011; Polvani et al. 2011b; Min and Son 2013; Tao et al. 2016), but could also be the result of the minimal observed warming in the Southern Ocean relative to the global average (Li et al. 2013; Armour et al. 2016; Hwang et al. 2017), which may act to strengthen the equator-to-pole temperature gradient, thereby strengthening thermal winds and shifting eddy-momentum flux convergence poleward in the SH (Lu et al. 2008).

By taking advantage of the long-term trend in  $PC_{\text{for}}$ , we estimated the time that the forced trend in Hadley Cell expansion would emerge above the probabilistic range of internally generated trends in the zonal mean and in the zonal varying sense. In the zonal mean, we showed that the forced trend may already be detectable above the noise level in the SH. This was due in part to the asymmetrical nature of the forced mode about the equator and the weaker projection of ENSO in the SH relative to the NH (Garreaud and Battisti 1999). In contrast, we showed that the zonal mean NH forced anomalies could require several more years at their

current trajectory to emerge above this noise level. These results were largely consistent when considering zonally varying P–E fields, but with the important exception of the North Atlantic. Here, the forced poleward shift in North Atlantic subtropical dry zones and mid-latitude storm tracks is mostly detectable above the noise (Fig. 6a, stipples).

One caveat is that these results are primarily based on a single model. GFDL-CM2.1 does not simulate the aerosol indirect effect, and therefore it is possible that aerosol related signals could be muted in this model. However, we achieved qualitatively similar results when repeating the Joint EOF with the Community Earth System Model (CESM) Large Ensemble (Kay et al. 2015), which does incorporate the aerosol indirect effect. We defer to future studies to evaluate the viability of these results in the full CMIP5 ensemble.

This study sheds light on several longstanding questions in the literature. For example, can atmospheric forcings and ENSO variations alone explain the observed changes in tropical width? The internal mode's relationship to ENSO is consistent with the emerging consensus in the literature that tropical expansion generated by a long-term transition from a more El Niño-like state (positive PDO) to a more La Niña-like state (negative PDO) could account for much of the observed trend since 1980 (Lu et al. 2008; Grassi et al. 2012; Allen et al. 2014; Lucas and Nguyen 2015; Mantsis et al. 2017; Allen and Kovilakam 2017). When we put our EOF modes into this observational context by comparing the combination of 1980–2013 changes in our forced and internal modes (Fig. 7a) to the regression of observed P–E with a composite edge index (Fig. 7b), we found that our EOF reconstruction qualitatively reproduced the large-scale observed drying of the global subtropics, the southward shift of the SH storm tracks, and much of the tropical anomalies, with the magnitude of the model anomalies falling within the range of observational uncertainty.

Consistent with recent studies of the hiatus, our results further reinforce the importance of accounting for both forced and internally driven variability when interpreting observed climate trends. Here we have focused exclusively on ENSO-driven variability, but other types of variability—e.g., the Annular Modes (Previdi and Liepert 2007) and the Atlantic Multidecadal Oscillation (AMO; Lucas and Nguyen 2015)—may also influence Hadley Cell width. However, it should be noted that our Joint EOF method does not identify these climate modes as major contributors to the interannual variability of Hadley Cell width, even in the higher order EOF modes.

Our study also raises the question of why the forced poleward shift in the storm tracks is stronger in the North Atlantic than elsewhere in the NH? Bender et al. (2012) also showed that the magnitude of the storm track shift was largest in the North Atlantic using satellite observations. Although they suggest this result should be viewed



with caution as data artifacts may spuriously amplify the observed trend, their conclusions imply that external forcings (rather than internal variability) may explain the bulk of the trend in this region. Aside from increased greenhouse gases, aerosol and tropospheric ozone forcings have also been suggested as drivers of forced Hadley Cell expansion in the SH (Kim et al. 2017) and in the North Atlantic (Allen et al. 2012; Kovilakam and Mahajan 2015). Since greenhouse gases, ozone, and aerosol forcings are not perfectly correlated during the historical period, it is difficult to assess the relative contributions of these climate forcings to tropical expansion when they are all included in a single mode (e.g., Fig. 1d–f). Therefore, targeted experiments that utilize single forcing simulations are needed to provide clarity on the role of individual forcings in North Atlantic Hadley Cell modes.

Finally, our results highlight just how unusual the period since 1980 has been. Based on Fig. 3b, observations suggest the 1980–2013 tropical Pacific cooling was exceptionally intense in the scope of modeled long-term natural variations. Consequently, this phase change substantially muted the global warming trend and generated accelerated Hadley Cell expansion. As the PDO cycle transitions to a warm phase, we expect the opposite to occur, with accelerated global warming and a “hiatus” in Hadley Cell expansion. On top of the additional contraction expected from ozone recovery (Polvani et al. 2011a), this suggests that the rapid pace of Hadley Cell expansion observed since 1980 will likely not be maintained through the first half of the twenty-first century.

**Acknowledgements** This material is based upon work supported in part by the National Science Foundation Graduate Research Fellowship (NSF; DGE-1144086). N. S. and S. P. X. are supported by the NSF (1637450). S. P. X. is further supported by the National Key R&D Program of China (2016YFA0601804). A. J. M is supported by the NSF (OCE1419306) and the National Oceanic and Atmospheric Administration (NOAA; NA14OAR4310276). We would like to thank Sarah M. Kang and Kristopher Karnauskas for their helpful comments during the course of our study. We also thank Yu Kosaka for running the additional 10-member GFDL-CM2.1 ensemble and the 1000-year control simulation. We also express our gratitude to the World Climate Research Programme’s Working Group on Coupled Modelling, which maintains CMIP. MERRA2 Reanalysis data was provided by the NASA Global Modeling and Assimilation Office, from their web site at <https://gmao.gsfc.nasa.gov/reanalysis/MERRA-2/>. Finally, we’d like to thank two anonymous reviewers for comments that improved the quality of this paper.

## References

- Allen RJ, Ajoku O (2016) Future aerosol reductions and widening of the northern tropical belt. *J Geophys Res Atmos* 121:6765–6786. doi:10.1002/2016JD024803
- Allen RJ, Kovilakam M (2017) The role of natural climate variability in recent tropical expansion. *J Clim* doi:10.1175/JCLI-D-16-0735.1
- Allen RJ, Sherwood SC, Norris JR, Zender CS (2012) Recent Northern Hemisphere tropical expansion primarily driven by black carbon and tropospheric ozone. *Nature* 485:350–354. doi:10.1038/nature11097
- Allen RJ, Norris JR, Kovilakam M (2014) Influence of anthropogenic aerosols and the Pacific Decadal Oscillation on tropical belt width. *Nat Geosci* 7:270–274. doi:10.1038/ngeo2091
- Amaya DJ, Xie SP, Miller AJ, McPhaden MJ (2015) Seasonality of tropical Pacific decadal trends associated with the 21st century global warming hiatus. *J Geophys Res Ocean* 120:6782–6798
- Archer CL, Caldeira K (2008) Historical trends in the jet streams. *Geophys Res Lett* 35:L08803. doi:10.1029/2008GL033614
- Armour KC, Marshall J, Scott JR et al (2016) Southern Ocean warming delayed by circumpolar upwelling and equatorward transport. *Nat Geosci* 9:549–554. doi:10.1038/ngeo2731
- Bender FAM, Ramanathan V, Tselioudis G (2012) Changes in extratropical storm track cloudiness 1983–2008: Observational support for a poleward shift. *Clim Dyn* 38:2037–2053. doi:10.1007/s00382-011-1065-6
- Cayan DR, Das T, Pierce DW et al (2010) Future dryness in the southwest US and the hydrology of the early 21st century drought. *Proc Natl Acad Sci* 107:21271–21276. doi:10.1073/pnas.0912391107
- Chen X, Wallace JM (2015) ENSO-like variability: 1900–2013. *J Clim* 28:9623–9641. doi:10.1175/JCLI-D-15-0322.1
- Chen S, Wei K, Chen W, Song L (2014) Regional changes in the annual mean hadley circulation in recent decades. *J Geophys Res* 119:7815–7832. doi:10.1002/2014JD021540
- Choi J, Son S-W, Lu J, Min S-K (2014) Further observational evidence of Hadley Cell widening in the Southern Hemisphere. *Geophys Res Lett*. doi:10.1002/2014GL059426
- CSIRO (Commonwealth Scientific and Industrial Research Organisation) (2012) Climate and water availability in South-Eastern Australia: a synthesis of findings from phase 2 of the South Eastern Australian climate initiative (SEACI). 41
- Davis NA, Birner T (2013) Seasonal to multidecadal variability of the width of the tropical belt. *J Geophys Res Atmos* 118:7773–7787. doi:10.1002/jgrd.50610
- Davis SM, Rosenlof KH (2012) A multidiagnostic intercomparison of tropical-width time series using reanalyses and satellite observations. *J Clim* 25:1061–1078. doi:10.1175/JCLI-D-11-00127.1
- Delworth TL, Broccoli AJ, Rosati A et al (2006) GFDL’s CM2 global coupled climate models. Part I: formulation and simulation characteristics. *J Clim* 19:643–674. doi:10.1175/JCLI3629.1
- Fu Q, Lin P (2011) Poleward shift of subtropical jets inferred from satellite-observed lower-stratospheric temperatures. *J Clim* 24:5597–5603. doi:10.1175/JCLI-D-11-00027.1
- Fyfe JC, Gillett NP (2014) Recent observed and simulated warming. *Nat Clim Chang* 4:150–151. doi:10.1038/nclimate2111
- Fyfe JC, Meehl GA, England MH et al (2016) Making sense of the early-2000s warming slowdown. *Nat Clim Chang* 6:224–228. doi:10.1038/nclimate2938
- Garfinkel CI, Waugh DW, Polvani LM (2015) Recent Hadley Cell expansion: the role of internal atmospheric variability in reconciling modeled and observed trends. *Geophys Res Lett* 42:10. doi:10.1002/2015GL066942
- Garreaud RD, Battisti DS (1999) Interannual (ENSO) and interdecadal (ENSO-like) variability in the Southern Hemisphere tropospheric circulation. *J Clim* 12:2113–2123. doi:10.1175/1520-0442(1999)012<2113:IEAIEL>2.0.CO;2
- Gelaro R, McCarty W, Suárez MJ et al (2017) The modern-era retrospective analysis for research and applications, version 2 (MERRA-2). *J Clim* 30(14):5419–5454
- Grassi B, Redaelli G, Canziani PO, Visconti G (2012) Effects of the PDO phase on the tropical belt width. *J Clim* 25:3282–3290. doi:10.1175/JCLI-D-11-00244.1

- Hansen J, Sato M, Kharecha P, Von Schuckmann K (2011) Earth's energy imbalance and implications. *Atmos Chem Phys* 11:13421–13449. doi:[10.5194/acp-11-13421-2011](https://doi.org/10.5194/acp-11-13421-2011)
- Hoerling M, Eischeid J, Perlwitz J et al (2012) On the increased frequency of mediterranean drought. *J Clim* 25:2146–2161. doi:[10.1175/JCLI-D-11-00296.1](https://doi.org/10.1175/JCLI-D-11-00296.1)
- Horel JD, Wallace JM (1981) Planetary-scale phenomena associated with the Southern Oscillation. *Mon Wea Rev* 109:813–829. doi:[10.1175/1520-0493\(1981\)109<0813:PSAPAW>2.0.CO;2](https://doi.org/10.1175/1520-0493(1981)109<0813:PSAPAW>2.0.CO;2)
- Hu Y, Fu Q (2007) Observed poleward expansion of the Hadley circulation since 1979. *Atmos Chem Phys Discuss* 7:9367–9384. doi:[10.5194/acpd-7-9367-2007](https://doi.org/10.5194/acpd-7-9367-2007)
- Hu Y, Tao L, Liu J (2013) Poleward expansion of the hadley circulation in CMIP5 simulations. *Adv Atmos Sci* 30:790–795. doi:[10.1007/s00376-012-2187-4](https://doi.org/10.1007/s00376-012-2187-4)
- Hwang Y-T, Xie S-P, Deser C, Kang SM (2017) Connecting tropical climate change with southern ocean heat uptake. *Geophys Res Lett* 44. doi:[10.1002/2017GL074972](https://doi.org/10.1002/2017GL074972)
- Johanson CM, Fu Q (2009) Hadley Cell widening: model simulations versus observations. *J Clim* 22:2713–2725. doi:[10.1175/2008JCLI2620.1](https://doi.org/10.1175/2008JCLI2620.1)
- Kang SM, Polvani LM, Fyfe JC, Sigmond M (2011) Impact of Polar Ozone Depletion on Subtropical Precipitation. *Science* 332:951–954. doi:[10.1126/science.1202131](https://doi.org/10.1126/science.1202131)
- Karnauskas KB, Ummenhofer CC (2014) On the dynamics of the Hadley circulation and subtropical drying. *Clim Dyn* 42:2259–2269. doi:[10.1007/s00382-014-2129-1](https://doi.org/10.1007/s00382-014-2129-1)
- Kay JE, et al. (2015) The community earth system model (CESM) large ensemble project: a community resource for studying climate change in the presence of internal climate variability. *Bull Am Meteorol Soc* 96:1333–1349. doi:[10.1175/BAMS-D-13-00255.1](https://doi.org/10.1175/BAMS-D-13-00255.1)
- Kim YH, Min SK, Son SW, Choi J (2017) Attribution of the local Hadley Cell widening in the Southern Hemisphere. *Geophys Res Lett* 44:1015–1024. doi:[10.1002/2016GL072353](https://doi.org/10.1002/2016GL072353)
- Kosaka Y, Xie S-P (2013) Recent global-warming hiatus tied to equatorial Pacific surface cooling. *Nature* 501:403–407. doi:[10.1038/nature12534](https://doi.org/10.1038/nature12534)
- Kosaka Y, Xie S-P (2016) The tropical Pacific as a key pacemaker of the variable rates of global warming. *Nat Geosci* 9:669–673. doi:[10.1038/ngeo2770](https://doi.org/10.1038/ngeo2770)
- Kovilakam M, Mahajan S (2015) Black carbon aerosol-induced Northern Hemisphere tropical expansion. *Geophys Res Lett* 42:4964–4972. doi:[10.1002/2015GL064559](https://doi.org/10.1002/2015GL064559)
- Li C, von Storch JS, Marotzke J (2013) Deep-ocean heat uptake and equilibrium climate response. *Clim Dyn* 40:1071–1086. doi:[10.1007/s00382-012-1350-z](https://doi.org/10.1007/s00382-012-1350-z)
- Lu J, Chen G, Frierson DMW (2008) Response of the zonal mean atmospheric circulation to El Niño versus global warming. *J Clim* 21:5835–5851. doi:[10.1175/2008JCLI2200.1](https://doi.org/10.1175/2008JCLI2200.1)
- Lucas C, Nguyen H (2015) Regional characteristics of tropical expansion and the role of climate variability. *J Geophys Res Atmos* 120:1–16. doi:[10.1002/2015JD023130](https://doi.org/10.1002/2015JD023130). Received
- Lucas C, Timbal B, Nguyen H (2014) The expanding tropics: a critical assessment of the observational and modeling studies. *Wiley Interdiscip Rev Clim Chang* 5:89–112. doi:[10.1002/wcc.251](https://doi.org/10.1002/wcc.251)
- Mantsis DF, Sherwood S, Allen RJ, Shi L (2017) Natural variations of tropical width and recent trends. *Geophys Res Lett*. doi:[10.1002/2016GL072097](https://doi.org/10.1002/2016GL072097)
- Min SK, Son SW (2013) Multimodel attribution of the Southern Hemisphere Hadley Cell widening: major role of ozone depletion. *J Geophys Res Atmos* 118:3007–3015. doi:[10.1002/jgrd.50232](https://doi.org/10.1002/jgrd.50232)
- Morales MS, Christie DA, Villalba R et al (2012) Precipitation changes in the South American Altiplano since 1300AD reconstructed by tree-rings. *Clim Past* 8:653–666. doi:[10.5194/cp-8-653-2012](https://doi.org/10.5194/cp-8-653-2012)
- Nguyen H, Evans A, Lucas C et al (2013) The hadley circulation in reanalyses: climatology, variability, and Change. *J Clim* 26:3357–3376. doi:[10.1175/JCLI-D-12-00224.1](https://doi.org/10.1175/JCLI-D-12-00224.1)
- Polvani LM, Previdi M, Deser C (2011a) Large cancellation, due to ozone recovery, of future Southern Hemisphere atmospheric circulation trends. *Geophys Res Lett*. doi:[10.1029/2011GL046712](https://doi.org/10.1029/2011GL046712)
- Polvani LM, Waugh DW, Correa GJP, Son S-W (2011b) Stratospheric ozone depletion: the main driver of twentieth-century atmospheric circulation changes in the southern hemisphere. *J Clim* 24:795–812. doi:[10.1175/2010JCLI3772.1](https://doi.org/10.1175/2010JCLI3772.1)
- Previdi M, Liepert BG (2007) Annular modes and Hadley Cell expansion under global warming. *Geophys Res Lett*. doi:[10.1029/2007GL031243](https://doi.org/10.1029/2007GL031243)
- Robinson WA (2002) On the midlatitude thermal response to tropical warmth. *Geophys Res Lett* 29:31. doi:[10.1029/2001GL014158](https://doi.org/10.1029/2001GL014158)
- Seager R, Harnik N, Kushnir Y, et al (2003) Mechanisms of hemispherically symmetric climate variability. *J Clim* 16:2960–2978. doi:[10.1175/1520-0442\(2003\)016<2960:MOHSCV>2.0.CO;2](https://doi.org/10.1175/1520-0442(2003)016<2960:MOHSCV>2.0.CO;2)
- Seager R, Naik N, Vecchi GA (2010) Thermodynamic and dynamic mechanisms for large-scale changes in the hydrological cycle in response to global warming. *J Clim* 23:4651–4668. doi:[10.1175/2010JCLI3655.1](https://doi.org/10.1175/2010JCLI3655.1)
- Seidel DJ, Randel WJ (2006) Variability and trends in the global tropopause estimated from radiosonde data. *J Geophys Res* 111:D21101. doi:[10.1029/2006JD007363](https://doi.org/10.1029/2006JD007363)
- Seidel D, Fu Q, Randel W, Reichler T (2008) Widening of the tropical belt in a changing climate. *Nat Geosci* 1:21–24. doi:[10.1038/ngeo.2007.38](https://doi.org/10.1038/ngeo.2007.38)
- Smith TM, Reynolds RW, Peterson TC, Lawrimore J (2008) Improvements to NOAA's historical merged land–ocean surface temperature analysis (1880–2006). *J Clim* 21:2283–2296. doi:[10.1175/2007JCLI2100.1](https://doi.org/10.1175/2007JCLI2100.1)
- Sousa PM, Trigo RM, Aizpurua P et al (2011) Trends and extremes of drought indices throughout the 20th century in the Mediterranean. *Nat Hazards Earth Syst Sci* 11:33–51. doi:[10.5194/nhess-11-33-2011](https://doi.org/10.5194/nhess-11-33-2011)
- Sterl A (2004) On the (in)homogeneity of reanalysis products. *J Clim* 17:3866–3873. doi:[10.1175/1520-0442\(2004\)017<3866:OTIORP>2.0.CO;2](https://doi.org/10.1175/1520-0442(2004)017<3866:OTIORP>2.0.CO;2)
- Stocker TF et al (2013) IPCC, 2013: Climate change 2013: the physical science basis. Contribution of Working Group I to the fifth assessment report of the Intergovernmental Panel on Climate Change. Cambridge University Press, Cambridge
- Takahashi C, Watanabe M (2016) Pacific trade winds accelerated by aerosol forcing over the past two decades. *Nat Clim Chang* 6:768–774. doi:[10.1038/nclimate2996](https://doi.org/10.1038/nclimate2996)
- Tao L, Hu Y, Liu J (2016) Anthropogenic forcing on the H circulation in CMIP5 simulations. *Clim Dyn* 46:3337–3350. doi:[10.1007/s00382-015-2772-1](https://doi.org/10.1007/s00382-015-2772-1)
- Trenberth KE, Stepaniak DP, Hurrell JW, et al (2001) Quality of reanalyses in the tropics. *J Clim* 14:1499–1510. doi:[10.1175/1520-0442\(2001\)014<1499:QORITT>2.0.CO;2](https://doi.org/10.1175/1520-0442(2001)014<1499:QORITT>2.0.CO;2)
- Wang H, Xie S-P, Tokinaga H et al (2016) Detecting cross-equatorial wind change as a fingerprint of climate response to anthropogenic aerosol forcing. *Geophys Res Lett* 43:3444–3450. doi:[10.1002/2016GL068521](https://doi.org/10.1002/2016GL068521)
- Watanabe M, Shiogama H, Tatebe H et al (2014) Contribution of natural decadal variability to global warming acceleration and hiatus. *Nat Clim Chang* 4:893–897. doi:[10.1038/nclimate2355](https://doi.org/10.1038/nclimate2355)
- Waugh DW, Garfinkel CI, Polvani LM et al (2015) Drivers of the recent tropical expansion in the southern hemisphere: changing SSTs or ozone depletion? *J Clim* 28:6581–6586. doi:[10.1175/JCLI-D-15-0138.1](https://doi.org/10.1175/JCLI-D-15-0138.1)

- WMO (World Meteorological Organization) (1957) Meteorology—a three-dimensional science. Second session of the Commission for Aerology. WMO Bulletin IV, no 4. WMO, Geneva, pp 134–138
- Xie S-P, Kosaka Y (2017) What caused the global surface warming hiatus of 1998–2013? *Curr Clim Chang Reports* 3:128–140. doi:[10.1007/s40641-017-0063-0](https://doi.org/10.1007/s40641-017-0063-0)
- Ye JS (2014) Trend and variability of China's summer precipitation during 1955–2008. *Int J Climatol* 34:559–566. doi:[10.1002/joc.3705](https://doi.org/10.1002/joc.3705)